A FEW-SHOT LABEL UNLEARNING IN VERTICAL FEDERATED LEARNING

Anonymous authors
Paper under double-blind review

ABSTRACT

This paper addresses the critical challenge of unlearning in Vertical Federated Learning (VFL), an area that has received limited attention compared to horizontal federated learning. We introduce the first approach specifically designed to tackle label unlearning in VFL, focusing on scenarios where the active party aims to mitigate the risk of label leakage. Our method leverages a limited amount of labeled data, utilizing manifold mixup to augment the forward embedding of insufficient data, followed by gradient ascent on the augmented embeddings to erase label information from the models. This combination of augmentation and gradient ascent enables high unlearning effectiveness while maintaining efficiency, completing the unlearning procedure within seconds. Extensive experiments conducted on diverse datasets, including MNIST, CIFAR10, CIFAR100, and ModelNet, validate the efficacy and scalability of our approach. This work represents a significant advancement in federated learning, addressing the unique challenges of unlearning in VFL while preserving both privacy and computational efficiency.

1 INTRODUCTION

Vertical Federated Learning (VFL) (Yang et al., 2019) allows multiple organizations to collaboratively utilize their private datasets in a privacy-preserving manner, even when they share some sample IDs but differ significantly in terms of features. In VFL, there are typically two types of parties: (i) the passive party, which holds the *features*, and (ii) the active party, which possesses the *labels*. VFL has seen widespread application, especially in sensitive domains like banking, healthcare, and e-commerce, where organizations benefit from joint modeling without exposing their raw data (Yang et al., 2019; Li et al., 2020).

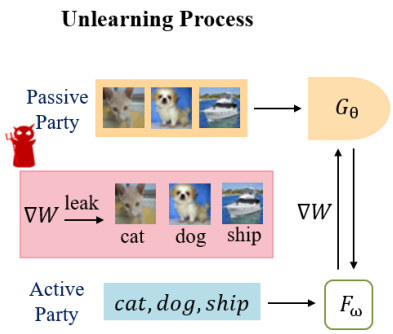

Figure 1: Illustration of risk of label leakage in vertical federated unlearning.

A fundamental requirement in VFL is the necessity for unlearning, which is driven by participants' "right to be forgotten" as mandated by regulations such as the General Data Protection Regulation (GDPR)[1] and the California Consumer Privacy Act (CCPA)[2]. While unlearning has been explored in the context of Horizontal Federated Learning (HFL), there has been limited attention to its application in vertical settings. Existing studies on vertical federated unlearning (Zhang et al., 2023a; Wang et al., 2024; Deng et al., 2023) primarily focus on the unlearning process for individual clients, often addressing the removal of all features from the passive party upon their exit. In contrast, this paper emphasizes the *unlearning of labels*, which is a critical aspect in VFL, particularly in scenarios such as Credit Risk Assessment where the determination of a loan applicant's likelihood of default is essential. Moreover, the active

[1] https://gdpr-info.eu/art-17-gdpr/
[2] https://oag.ca.gov/privacy/ccpa

party aims to eliminate label information not only from the active model but also from the passive models, as the passive models may retain label information (Fu et al., 2022b).

A significant challenge in directly applying traditional machine unlearning methods, such as retraining (Bourtoule et al., 2020; Foster et al., 2023) or Boundary unlearning (Chen et al., 2023), in this context pose a *risk of leaking unlearned labels* during the unlearning process. Typically, the active party, which retains the labels, must either inform the passive party about the samples that require unlearning or transfer the gradients associated with the unlearned label. This practice may inadvertently expose sensitive label information to the passive party (see Fig. 1 and Sect. 3.2).

To address this challenge, we propose a few-shot unlearning method that effectively erases labels from both the active model and passive model in VFL by leveraging a limited amount of private data (see Sect. 4). Specifically, our method employs manifold mixup (Verma et al., 2019) to augment the forward embeddings of each passive party. The active party then performs gradient ascent on the mixed embeddings to unlearn the active model and subsequently transfers the inverse gradients to the passive party to facilitate the unlearning of the passive model independently. This approach offers three key advantages: first, it necessitates only labels from a small amount of private data, significantly reducing the risk of label privacy leakage; second, by utilizing the manifold mixup technique, it enhances unlearning effectiveness with minimal data; and third, it is highly efficient, completing the unlearning process within seconds.

The primary contributions of this work are as follows:

1. To the best knowledge, this is the first work to address the unlearning of labels in VFL.
2. We systematically elucidate the label privacy leakage that may occur when directly applying traditional machine unlearning methods in Sect. 3.2.
3. We propose a few-shot label unlearning method that effectively erases labels from both the active and passive models in VFL, utilizing a limited amount of private data. Moreover, this approach leverages only a small number of data to mitigate the risk of label privacy leakage while employing manifold mixup to enhance unlearning effectiveness.
4. We conduct extensive experiments on multiple benchmark datasets, including MNIST, CIFAR-10, CIFAR-100, and ModelNet, demonstrating that our method rapidly and effectively unlearns target labels compared to other machine unlearning methods.

2 Related Works

Machine Unlearning & Horizontal Federated Unlearning. Machine unlearning (MU) was initially introduced by (Cao & Yang, 2015) to selectively remove some data from model without retrain the model from scratch (Garg et al., 2020; Chen et al., 2021). MU can be categorized into exact unlearning and approximate unlearning. Exact unlearning methods such as SISA (Bourtoule et al., 2020) and ARCANE (Yan et al., 2022) split data into sections and train sub-models for each data section and merge all sub-models. During unlearning, retrain the affected data section and merge all sub-models again. In approximate unlearning, techniques such as fine tuning (Golatkar et al., 2020a; Jia et al., 2024) (fine tune with $\mathcal{D}_r$), random label (Graves et al., 2020; Chen et al., 2023) (fine tune with incorrect random label of $\mathcal{D}_u$), noise introducing (Tarun et al., 2024; Huang et al., 2021), gradient ascent (Goel et al., 2023; Choi & Na, 2023; Abbasi et al., 2023; Hoang et al., 2023) (maximise loss associate with $\mathcal{D}_u$), knowledge distillation (Chundawat et al., 2023; Zhang et al., 2023c; Kurmanji et al., 2023) (train a student model) and weights scrubbing (Golatkar et al., 2020a;b; 2021; Guo et al., 2023; Foster et al., 2023) (discarding heavily influenced weights) are used.

Meanwhile, in federated unlearning, most of the existing works are focused in the horizontal environment (Wu et al., 2022; Gu et al., 2024a; Zhao et al., 2024a; Romandini et al., 2024; Liu et al., 2024; Zhang et al., 2023b; Su & Li, 2023; Ye et al., 2023; Gao et al., 2022; Cao et al., 2022; Yuan et al., 2022; Alam et al., 2023; Li et al., 2023; Halimi et al., 2023; Xia et al., 2023; Wang et al., 2023; Dhasade et al., 2023; Liu et al., 2022; Zhao et al., 2024b; Wang et al., 2022; Gu et al., 2024b). Only very limited research works focus in the vertical environment. For instance, (Zhang et al., 2023a) introduce vertical federated unlearning (VFU) in gradient boosting tree. (Wang et al., 2024) introduce passive party unlearning on deep learning model with fast retraining on remaining parties, and (Deng et al., 2023) introduce passive party unlearning on logistic regression model.

Most if not all existing VFU work have been primarily focused on passive parties unlearning (Zhang et al., 2023a; Wang et al., 2024; Deng et al., 2023). Hence, a significant gap arise when an active party seeks for a collaboration from passive parties for a single class unlearning while all parties remaining engaged in VFL. Unfortunately, current VFU approaches do not address this specific scenario, as they do not explore class unlearning within VFL setting. In contrast to prior works focusing on class unlearning in centralise machine unlearning and horizontal federated unlearning settings, this paper uniquely addresses class unlearning of classification model within the VFL paradigm. This distinction arises because traditional class unlearning methods in centralised and horizontal federated learning setting are impractical for VFL settings, where all parties have different features of data and different computational power.

Vertical Federated Learning & Privacy Leakage. VFL is introduced to meet the needs of enterprises looking to utilize features distributed across multiple parties for improved model performance, compared to models trained by a single entity, all while preserving data privacy (Yang et al., 2019). In VFL, privacy is of utmost importance because the participants are typically companies that handle valuable and sensitive user information. Hence, privacy protection during VFU is also an important criteria. We explain the risk of label leakage during VFU in Sect. 3.2.

3 Label Leakage during Vertical Federated Unlearning

This section explains the risk of label leakage during label unlearning process as depicted in Fig. 1.

3.1 General Setup

VFL Training. We assume that a VFL setting consists of one active party P_0 and K passive parties $\{P_1, \cdots, P_K\}$ who collaboratively train a VFL model $\Theta = (\theta, \omega)$ to optimize:

$$\min_{\omega,\theta_1,\cdots,\theta_K} \frac{1}{n} \sum_{i=1}^{n} \ell(F_\omega \circ (G_{\theta_1}(x_{1,i}), G_{\theta_2}(x_{2,i}), \cdots, G_{\theta_K}(x_{K,i})), y_i), \tag{1}$$

in which Party P_k owns features $\mathbf{x}_k = (x_{k,1}, \cdots, x_{k,n})$ and the passive model G_{θ_k}, the active party owns the labels $\mathbf{y} = \{y_1, \cdots, y_m\}$ and active model F_ω. Each passive party k transfers its forward embedding H_k to the active party to compute the loss. The active model F_ω and passive models $G_{\theta_k}, k \in \{1, \ldots, K\}$ are trained based on backward gradients. Note that, before training, all parties leverage Private Set Intersection (PSI) protocols to align data records with the same IDs.

Unlearning Label in VFL. When the active party requests to unlearn some sensitive labels $\mathbf{y}^u$, where the corresponding unlearn feature is $\{\mathbf{x}_k^u\}_{k=1}^K := \{\{x_{k,i}^u\}_{i=1}^{n_u}\}_{k=1}^K$. The active party aims to remove the influence of $\mathbf{y}^u$ on both the active model F_ω and K passive models $\{G_{\theta_k}\}_{k=1}^K$.

Label unlearning in VFL refers to the process of efficiently and securely removing label information from a VFL system. Specifically, the unlearned passive model, denoted as θ^u, and the unlearned active model, denoted as ω^u, are obtained through the application of an unlearning mechanism $\mathcal{U}$, as follows:

$$\theta^u = \mathcal{U}(\theta, g_u), \quad \omega^u = \mathcal{U}(\omega, y_u),$$

where θ and ω represent the passive and active models before unlearning, respectively, and g_u are the gradients associated with the unlearned label y_u.

Building upon the principles of machine unlearning presented in (Bourtoule et al., 2020), label unlearning in VFL needs to satisfy the following three objectives: i) **Selective Removal**: The influence of specific labels must be erased while preserving the integrity of other data. ii) **Efficiency**: The unlearning process should achieve the above without requiring the computational cost of retraining the model from scratch. iii) **Privacy Preservation**: The unlearning process must ensure that no sensitive label information is leaked to the passive party.

Threat Model. We assume all participating parties are *semi-honest* and do not collude with each other. An adversary (i.e., the passive party) faithfully executes the training protocol but may launch privacy attacks to infer the private labels of the active party.

Assumption. We assume that the passive party possesses corresponding labels for a limited number of features, defined as $\mathcal{D}^p = \{(\mathbf{x}_k^p, \mathbf{y}^p)\}_{k=1}^K = \{\{(x_{k,i}^p, y_i)\}_{i=1}^{n_p}\}_{k=1}^K$, where $n_p << n_u$. This assumption is reasonable, as the active party must convey some label information to the passive party in order to effectively remove that information. Furthermore, this assumption is widely employed in prior works (Fu et al., 2022b; Gu et al., 2023; Zou et al., 2022).

3.2 Label leakage during unlearning

To remove the influence of the passive models $\{G_{\theta_k}\}_{k=1}^K$, there exists a risk of unlearning label leakage ($\mathbf{y}_u = \{y_1^u, \ldots, y_{m_u}^u\}$) to the passive parties. During the unlearning process, the active party is required to transfer information to the passive party, e.g., gradients $\mathbf{g}_u = \{g_1^u, \ldots, g_{n_u}^u\}$, in order to effectively unlearn the label associated with the passive model. Consequently, the passive party may infer the label based on this information.

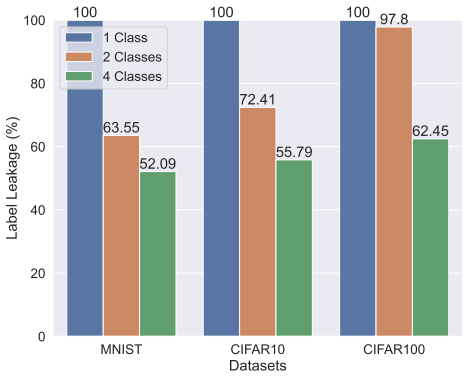

Figure 2: Illustration of label leakage accuracy during Boundary unlearning in VFL using ResNet18 model with different number of classes.

In particular, when unlearning a single class $y_{u,1}$, we consider two representative unlearning methods: (i) retraining (Foster et al., 2023) and (ii) Boundary unlearning (Chen et al., 2023). For retraining methods, the active party must inform the passive party regarding which features do not require training, thus, the label is leaked. In the case of Boundary unlearning, the gradients transferred to the passive party correspond to the features associated with the label $y_{u,1}$ may leak the label.

Furthermore, when multiple labels (m_u) are targeted for unlearning, the label leakage issue becomes exacerbated. Lets consider the Boundary unlearning as an example. This method illustrates that the passive party can infer label information from the gradients $\mathbf{g}_u$ transmitted by the active party during the unlearning process. Specifically, the passive party employs clustering on $\mathbf{g}_u$ to derive m_u clusters by optimizing the following objective function:

$$\min \sum_{g_i \in \mathcal{C}_j} \sum_{j=1}^{m_u} |g_{u,i} - \bar{g}_{u,j}|, \tag{2}$$

where $\mathcal{C}_j$ denotes the set of points assigned to cluster j, and $\bar{g}_{u,j}$ represents the centroid of cluster j. Consequently, the passive party can deduce the labels of the features in $\mathcal{X}$. Fig. 2 exposes the label leakage (in %) during unlearning in VFL for varying numbers of unlearning classes. For instance, with four classes from CIFAR-100, the passive party achieves a clustering accuracy of 62.45%.

4 The Proposed few-shot label unlearning method

This section details the proposed few-shot label unlearning method as illustrated in Fig. 3 and Algorithm 1. Our solution comprises two primary steps: first, augmenting the forward embedding through manifold mixup to address the scarcity of labeled data for unlearning (see Sect. 4.1). Second, employing gradient ascent on the augmented embedding to influence both the passive and active models, thereby facilitating the removal of the specified class, as elaborated in Sect. 4.2.

4.1 Vertical Manifold Mixup

Due to the label privacy leakage issue (Sect. 3.2), directly applying traditional machine unlearning methods will pose some challenges. We assume that the active party discloses a limited number of labels to the passive party to facilitate the unlearning of a specific class. However, this small labeled

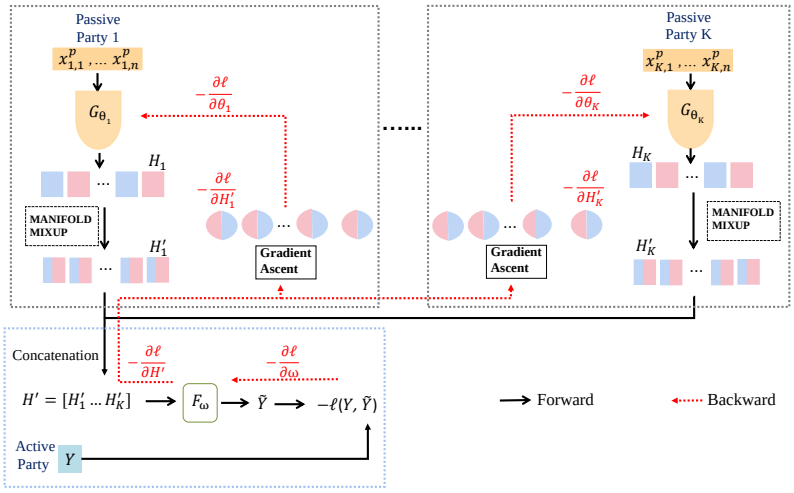

Figure 3: Overview of our proposed few-shot unlearning framework in VFL setting.

dataset, denoted as $\mathcal{D}_p$, is insufficient for an effective unlearning (see Appendix). Consequently, this scenario can be framed as a few-shot unlearning problem, wherein a minimal set of labels is employed to unlearn all associated labels.

Drawing inspiration from the few-shot learning principles, we adopt the manifold mixup mechanism (Verma et al., 2019) by interpolating hidden embeddings rather than directly mixing the features. We propose a manifold mixup framework for VFL by optimizing the following loss function:

$$\min_{\omega,\theta_1,\cdots,\theta_K} \frac{1}{n_p^2} \sum_{i,j=1}^{n_p} \ell(F_\omega \circ (\text{Mix}_\lambda(G_{\theta_1}(x_{1,i}^p), G_{\theta_1}(x_{1,j}^p)), \cdots, \text{Mix}_\lambda(G_{\theta_K}(x_{K,i}^p), G_{\theta_K}(x_{K,j}^p)), \text{Mix}_\lambda(y_i^p, y_j^p)),$$

where

$$\text{Mix}_\lambda(a,b) = \lambda \cdot a + (1-\lambda) \cdot b. \tag{3}$$

The mixed coefficient λ ranges from 0 to 1. The advantage of the manifold mixup approach lies in its ability to flatten the state distributions (Verma et al., 2019). Specifically, for each passive party k, mixup is applied to the forward embeddings $\{H_k^p = G_\theta(x_{k,i}^p)\}$ to generate numerous mixed embeddings H_k'. Subsequently, all passive parties transfer their respective mixed embeddings H_k' to the active party.

Algorithm 1 Our Method

Input: Bottom models parameters θ_k of K passive parties, top model parameters ω , unlearn data $\mathcal{D}_u$, learning rate η, unlearn epoch N.
Output: Unlearned bottom models parameters θ_k^u, unlearned top model parameters ω^u

for n in N **do**:
  for (x_i^u, y_i^u) in $\mathcal{D}_u$ **do**:
    ▷ *Passive parties k:*
    Split x_i^u to K parts.
    for $k = 1$ to K **do**:
      $H_k = G_{\theta_k}(x_{k,i}^u)$
      Generate H_k' from H_k according to equation 3.
    ▷ *Active party:*
    $H' = [H_1', ..., H_K']$.
    $y = F_\omega(H')$.
    $L = \ell(y, y')$.
    $\omega = \omega + \eta \cdot \frac{\partial L}{\partial \omega}$
    Active party compute $\frac{\partial \ell}{\partial H_k'}$ to transfer all passive parties.
    ▷ *Passive parties k:*
    for $k = 1$ to K **do**:
      $g_k = \frac{\partial \ell}{\partial H_k'} \cdot \frac{\partial H_k}{\partial \omega}$
      $\theta_k = \theta_k + \eta \cdot g_k$
Return θ_k^u and ω^u.

4.2 Vertical Label Unlearning via Gradient Ascent

Once the augmented embeddings $\{H_1', \ldots, H_K'\}$ for the representative unlearned data $\mathcal{D}_p$ (label is known) are generated, a straightforward yet effective strategy is to implement gradient ascent for both the active and passive models using these augmented embeddings. Specifically, the active party concatenates all embeddings $\{H_k'\}_{k=1}^K$ into a single tensor $H' = [H_1', \ldots, H_K']$, and optimizes it according to the following formulation:

$$\min_\omega \ell(F_\omega(H'), y') = \ell(F_\omega([H_1', \ldots, H_K']), y'), \tag{4}$$

where y' represents the mixture of the representative unlearned labels and η is the learning rate.

Unlearning for active model F_ω. On one hand, the active model undergoes unlearning for active model F_ω via gradient ascent as follows:

$$\omega = \omega + \eta \nabla_\omega \ell(F_\omega(H'), y'). \tag{5}$$

Unlearning for passive model G_{ω_k}. Subsequently, the active party computes the gradients $g'_k = \frac{\partial \ell}{\partial H'_k}$ in accordance with equation 4 and transmits these gradients to the corresponding passive party k. Finally, the passive party k updates the passive model G_{θ_k} using the following expression:

$$\theta_k = \theta_k + \eta \nabla_{H'_k} \ell(F_\omega(H'), y') \cdot \nabla_{\theta_k} H'_k. \tag{6}$$

It is important to note that gradient ascent may lead to significant degradation in model utility or even result in vanishing gradients if the parameters are not appropriately tuned. Therefore, employing a small learning rate η and a limited number of unlearning epochs can mitigate these issues while achieving effective unlearning results (see experimental details in Appendix A).

5 Experimental Results

This section presents the empirical analysis of the proposed method in terms of utility, unlearning effectiveness, time efficiency and some ablation studies.

5.1 Experiment Setup

Unlearning Scenarios *Single-class unlearning*: We forget a single class from all datasets. *Two-classes unlearning*: We forget two classes from CIFAR10 and CIFAR100. *Multi-classes unlearning*: We forget four classes from CIFAR100.

VFL Setting & Datasets & Models We stimulate a VFL scenario by splitting a neural network into two bottom models and a top model and assigning the two bottom models to each two passive parties and the top model to the active party. We conduct experiments on four datasets: MNIST (Lecun et al., 1998), CIFAR10, CIFAR100 (Krizhevsky et al., 2009) and ModelNet (Wu et al., 2015). We adopt Resnet18 (He et al., 2015) on dataset MNIST, CIFAR10, CIFAR100 and ModelNet. We do extend our experiments with Vgg16 (Simonyan & Zisserman, 2015) on dataset CIFAR10 and CIFAR100. Experiments are repeated over five random trials, and results are reported as mean and standard deviation. Further details are in Appendix A.3.

Evaluations Metrics We evaluate the utility of unlearning by measuring accuracy of $\mathcal{D}_r$ before and after unlearning. The higher accuracy on $\mathcal{D}_r$ indicates stronger utility. To evaluate the unlearning effectiveness, we construct a simple MIA from (Shokri et al., 2017) to test Attack Success Rate (ASR) and measuring the accuracy of $\mathcal{D}_u$ before and after unlearning. MIA seeks to determine if a specific data record was included in the training of a target machine learning model. Time efficiency is evaluated by comparing the runtime of each baseline.

Baselines We compare our method with the following baselines: Retrain, Fine Tuning (Golatkar et al., 2020a; Jia et al., 2024), Fisher Forgetting (Golatkar et al., 2020a), Amnesiac Unlearning (Graves et al., 2020), UNSIR (Tarun et al., 2024) and Boundary Unlearning (Chen et al., 2023). Additional details are available in Appendix A.3.

5.2 Experimental Results

5.2.1 Utility Guarantee

To assess the utility of our proposed unlearning method, we evaluate accuracy on $\mathcal{D}_r$ before and after unlearning (Tab. 1, 2, 3). An effective unlearning method should retain as much information as possible from $\mathcal{D}_r$.

From Tab. 1, 2, 3, we observe that: i) Fine-tuning achieves good preservation on $\mathcal{D}_r$, but its unlearning effectiveness is low (see Sect. 5.2.2). ii) Fisher forgetting badly preserves the information

Model	Datasets	Metrics	Accuracy (%)							
			Baseline	Retrain	FT	Fisher	Amnesiac	Unsir	BU	Ours
Resnet18	MNIST	$\mathcal{D}_r$	99.29	99.33 ± 0.03	**98.99 ± 0.05**	12.16 ± 0.46	98.16 ± 0.92	84.92 ± 1.13	98.72 ± 0.02	98.89 ± 0.00
		$\mathcal{D}_u$	99.39	0.00 ± 0.00	**0.00 ± 0.00**	**0.00 ± 0.00**	**0.00 ± 0.00**	**0.00 ± 0.00**	58.83 ± 1.79	**0.00 ± 0.00**
		ASR	90.61	1.03 ± 0.24	2.92 ± 1.08	0.11 ± 0.07	0.00 ± 0.00	29.07 ± 7.95	0.47 ± 0.01	0.63 ± 0.01
	CIFAR10	$\mathcal{D}_r$	90.61	91.26 ± 0.12	88.16 ± 0.15	54.4 ± 10.77	86.37 ± 0.20	75.02 ± 1.65	72.65 ± 0.55	**89.11 ± 0.14**
		$\mathcal{D}_u$	93.10	0.00 ± 0.00	11.00 ± 0.10	**0.00 ± 0.00**	**0.00 ± 0.00**	**0.00 ± 0.00**	3.25 ± 0.15	**0.00 ± 0.00**
		ASR	83.84	25.98 ± 1.27	15.85 ± 2.33	50.67 ± 12.51	1.62 ± 0.54	76.78 ± 0.44	34.90 ± 1.16	16.21 ± 0.63
	CIFAR100	$\mathcal{D}_r$	71.43	71.03 ± 0.12	66.86 ± 0.73	61.04 ± 8.61	60.05 ± 0.03	59.32 ± 0.14	55.30 ± 0.81	**67.85 ± 0.03**
		$\mathcal{D}_u$	83.00	0.00 ± 0.00	12.25 ± 2.25	**0.00 ± 0.00**	**0.00 ± 0.00**	**0.00 ± 0.00**	3.50 ± 0.50	**0.00 ± 0.00**
		ASR	88.40	25.53 ± 3.36	29.30 ± 2.70	28.10 ± 4.10	2.60 ± 1.30	73.70 ± 1.70	6.00 ± 0.60	13.47 ± 0.19
	ModelNet	$\mathcal{D}_r$	94.26	93.90 ± 0.11	66.64 ± 1.53	28.10 ± 0.69	73.91 ± 1.83	13.51 ± 0.05	24.07 ± 0.27	**83.32 ± 0.07**
		$\mathcal{D}_u$	100.00	0.00 ± 0.00	**0.00 ± 0.00**	**0.00 ± 0.00**	**0.00 ± 0.00**	**0.00 ± 0.00**	**0.00 ± 0.00**	2.00 ± 0.00
		ASR	98.40	0.65 ± 0.05	0.79 ± 0.16	23.48 ± 0.77	1.11 ± 0.16	49.20 ± 1.25	21.16 ± 0.23	0.46 ± 0.07
Vgg16	CIFAR10	$\mathcal{D}_r$	89.50	90.27 ± 0.19	88.69 ± 0.08	15.93 ± 4.82	84.67 ± 0.22	74.74 ± 0.72	82.69 ± 0.1	**88.85 ± 0.24**
		$\mathcal{D}_u$	91.10	0.00 ± 0.00	4.25 ± 1.05	**0.00 ± 0.00**	**0.00 ± 0.00**	**0.00 ± 0.00**	2.85 ± 0.05	1.60 ± 0.16
		ASR	81.66	33.10 ± 1.86	21.84 ± 2.66	42.25 ± 6.23	2.36 ± 0.86	21.75 ± 2.41	34.53 ± 0.65	31.59 ± 0.34
	CIFAR100	$\mathcal{D}_r$	65.48	65.32 ± 0.32	59.92 ± 0.56	35.42 ± 1.95	55.83 ± 0.13	55.78 ± 0.59	52.21 ± 0.00	**62.13 ± 0.06**
		$\mathcal{D}_u$	77.00	0.00 ± 0.00	2.50 ± 0.25	**0.00 ± 0.00**	**0.00 ± 0.00**	**0.00 ± 0.00**	3.00 ± 0.00	4.30 ± 0.94
		ASR	87.20	42.13 ± 2.73	34.50 ± 4.30	40.70 ± 3.50	3.10 ± 0.15	42.70 ± 0.70	18.20 ± 0.11	21.73 ± 0.84

Table 1: Accuracy of $\mathcal{D}_r$ and $\mathcal{D}_u$ for each unlearning method across Resnet18 and Vgg16 model in single-class unlearning

Model	Datasets	Metrics	Accuracy (%)							
			Baseline	Retrain	FT	Fisher	Amnesiac	Unsir	BU	Ours
Resnet18	CIFAR10	$\mathcal{D}_r$	91.48	91.74 ± 0.01	**90.63 ± 0.57**	31.25 ± 2.23	86.16 ± 0.82	74.48 ± 0.06	81.64 ± 0.56	88.25 ± 0.09
		$\mathcal{D}_u$	88.40	0.00 ± 0.00	41.15 ± 1.55	49.55 ± 0.40	**0.00 ± 0.00**	**0.00 ± 0.00**	19.90 ± 0.85	0.63 ± 0.60
		ASR	79.61	21.66 ± 0.64	13.22 ± 0.37	25.60 ± 0.08	1.84 ± 0.13	41.79 ± 1.35	35.40 ± 1.54	28.20 ± 1.48
	CIFAR100	$\mathcal{D}_r$	71.56	71.21 ± 0.13	66.04 ± 0.58	53.56 ± 2.54	59.52 ± 0.03	58.02 ± 0.37	56.37 ± 0.39	**66.89 ± 0.05**
		$\mathcal{D}_u$	71.00	0.00 ± 0.00	38.00 ± 0.01	25.20 ± 5.75	**0.00 ± 0.00**	**0.00 ± 0.00**	13.00 ± 0.01	6.50 ± 0.71
		ASR	88.60	21.60 ± 0.85	19.20 ± 1.20	48.90 ± 0.54	6.50 ± 0.40	54.83 ± 0.44	13.70 ± 0.90	6.50 ± 0.33
Vgg16	CIFAR10	$\mathcal{D}_r$	89.80	91.13 ± 0.03	88.09 ± 0.35	47.53 ± 2.38	86.16 ± 0.19	71.50 ± 0.07	88.67 ± 0.22	**88.21 ± 0.02**
		$\mathcal{D}_u$	89.10	0.00 ± 0.00	28.55 ± 0.33	13.10 ± 0.28	**0.00 ± 0.00**	**0.00 ± 0.00**	19.08 ± 0.53	**0.00 ± 0.00**
		ASR	82.64	28.31 ± 1.23	17.75 ± 2.22	68.43 ± 1.14	1.67 ± 0.01	46.21 ± 0.72	11.72 ± 0.07	28.37 ± 0.86
	CIFAR100	$\mathcal{D}_r$	65.75	65.59 ± 0.17	60.79 ± 0.37	35.24 ± 2.21	57.86 ± 0.81	56.04 ± 0.44	50.02 ± 0.18	**62.49 ± 0.11**
		$\mathcal{D}_u$	58.50	0.00 ± 0.00	11.75 ± 1.25	11.00 ± 4.85	**0.00 ± 0.00**	**0.00 ± 0.00**	3.25 ± 0.25	**0.00 ± 0.00**
		ASR	73.60	30.55 ± 0.05	22.75 ± 1.05	32.60 ± 1.17	3.45 ± 0.65	52.40 ± 0.80	27.90 ± 1.20	30.60 ± 1.80

Table 2: Accuracy of $\mathcal{D}_r$ and $\mathcal{D}_u$ for each unlearning method across Resnet18 and Vgg16 model in two-classes unlearning

of $\mathcal{D}_r$, resulting in a huge degradation on $\mathcal{D}_r$ accuracy. iii) Random incorrect labeling of $\mathcal{D}_u$ from Amnesiac Unlearning causes the decision boundaries of $\mathcal{D}_r$ to shift unpredictably, resulting in a drop in accuracy on $\mathcal{D}_r$. This degradation is more pronounced in datasets with a large number of classes, such as CIFAR100 and ModelNet. iv) The repair step from UNSIR fails to fully retain the information in $\mathcal{D}_r$, leading to some performances degradation on $\mathcal{D}_r$. v) Boundary unlearning exhibits inconsistencies across different datasets, models, and scenarios. In some cases, they show huge degradation on $\mathcal{D}_r$, while in other instances, they preserve $\mathcal{D}_r$ well. Contrary, vi) our solution shows good unlearning utility in all experiment settings.

5.2.2 Unlearning Effectiveness

For unlearning effectiveness, we run MIA to evaluate if the unlearned model leaks any information about the $\mathcal{D}_u$ and measure the accuracy of $\mathcal{D}_u$ before and after unlearning.

From Tab. 1, 2, 3, we observe that: i) Fine-tuning shows bad unlearning effectiveness on CIFAR10/100 datasets. The unlearning effectiveness of fine tuning is worse on two-classes (Tab. 2) and multi-classes unlearning scenarios (Tab. 3); ii) Fisher forgetting, Amnesiac Unlearning and UNSIR show strong unlearning effectiveness, reducing accuracy of $\mathcal{D}_u$ to 0.00%; iii) Boundary unlearning exhibits inconsistencies across different datasets, models, and scenarios. In some cases, they show good unlearning effectiveness on $\mathcal{D}_u$, while in other instances, they show bad unlearning effectiveness. In contrast, iv) our solution demonstrates strong effectiveness across all models, datasets, and scenarios. It achieves successful unlearning of $\mathcal{D}_u$.

Model	Datasets	Metrics	Accuracy (%)							
			Baseline	Retrain	FT	Fisher	Amnesiac	Unsir	BU	Ours
Resnet18	CIFAR100	$\mathcal{D}_r$	71.53	71.91 ± 0.12	67.16 ± 0.13	54.79 ± 1.04	59.09 ± 0.54	59.05 ± 0.38	48.96 ± 0.04	**69.87 ± 0.09**
		$\mathcal{D}_u$	72.00	0.00 ± 0.00	33.87 ± 0.88	45.38 ± 1.13	**0.00 ± 0.00**	**0.00 ± 0.00**	15.00 ± 0.25	4.83 ± 1.12
		ASR	86.65	16.95 ± 0.35	18.23 ± 1.63	62.78 ± 3.93	6.05 ± 1.19	68.63 ± 1.83	38.35 ± 0.75	13.97 ± 0.45
Vgg16	CIFAR100	$\mathcal{D}_r$	65.83	65.66 ± 0.08	60.92 ± 0.08	36.55 ± 1.07	57.26 ± 0.18	56.86 ± 0.26	47.04 ± 0.32	**64.33 ± 0.16**
		$\mathcal{D}_u$	60.25	0.00 ± 0.00	7.63, 0.13	28.75 ± 1.25	**0.00 ± 0.00**	**0.00 ± 0.00**	7.13 ± 0.11	6.00 ± 0.25
		ASR	75.80	27.20 ± 0.75	24.38 ± 3.13	55.20 ± 3.75	4.80 ± 0.05	32.83 ± 0.58	29.70 ± 0.03	27.50 ± 0.65

Table 3: Accuracy of $\mathcal{D}_r$ and $\mathcal{D}_u$ for each unlearning method across Resnet18 and Vgg16 model in multi-classes unlearning

Number of Passive Parties	Metrics	Accuracy (%)							
		Baseline	Retrain	FT	Fisher	Amnesiac	Unsir	BU	Ours
1	$\mathcal{D}_r$	92.50	93.27 ± 0.11	88.51 ± 0.09	76.83 ± 3.02	88.95 ± 0.58	77.89 ± 0.48	89.66 ± 0.08	**90.01 ± 0.46**
	$\mathcal{D}_u$	93.60	0.00 ± 0.00	**0.00 ± 0.00**	**0.00 ± 0.00**	**0.00 ± 0.00**	**0.00 ± 0.00**	23.60 ± 1.60	**0.00 ± 0.00**
	ASR	89.34	24.54 ± 1.38	40.27 ± 3.15	66.40 ± 1.98	0.36 ± 0.14	15.83 ± 0.49	19.66 ± 0.56	16.13 ± 0.36
2	$\mathcal{D}_r$	90.61	91.26 ± 0.12	88.16 ± 0.15	54.40 ± 10.77	86.37 ± 0.20	75.02 ± 1.65	72.65 ± 0.55	**89.11 ± 0.14**
	$\mathcal{D}_u$	93.10	0.00 ± 0.00	11.00 ± 0.10	**0.00 ± 0.00**	**0.00 ± 0.00**	**0.00 ± 0.00**	3.25 ± 0.15	**0.00 ± 0.00**
	ASR	83.84	25.98 ± 1.27	15.85 ± 2.33	50.67 ± 12.51	1.62 ± 0.54	76.78 ± 0.44	34.90 ± 1.16	16.21 ± 0.63
4	$\mathcal{D}_r$	88.12	89.04 ± 0.02	77.52 ± 1.15	41.56 ± 0.49	81.77 ± 0.04	71.88 ± 0.39	73.85 ± 0.49	**86.69 ± 0.13**
	$\mathcal{D}_u$	91.40	0.00 ± 0.00	**0.00 ± 0.00**	**0.90, 0.00**	**0.00 ± 0.00**	**0.00 ± 0.00**	1.81 ± 0.03	**0.00 ± 0.00**
	ASR	79.58	25.86 ± 2.04	63.44 ± 0.44	52.05 ± 0.91	2.90 ± 0.38	76.52 ± 4.16	72.61 ± 0.97	21.51 ± 0.69

Table 4: Accuracy of $\mathcal{D}_r$ and $\mathcal{D}_u$ for each unlearning method across Resnet18 model in single-class unlearning on different number of passive parties.

Also, on the same tables (Tab. 1-3), we observe that: i) Fine tuning shows consistent ASR score. ii) Fisher forgetting shows high ASR score in most of the cases. iii) Amnesiac unlearning shows inconsistencies in ASR score across all experiments. iv) UNSIR shows high ASR score on almost all experiments, v) Boundary unlearning shows relatively consistent ASR scores. Finally, all in all vi) our solution shows a consistent ASR performance across all datasets, models and scenarios.

5.2.3 Time Efficiency

For the computational complexity, Fig. 4 presents an execution time (in seconds) of single-class unlearning with Resnet18 model in CIFAR10 dataset. It can be observed that: i) The gold standard retrain model has the highest execution time. ii) Unlearning methods that utilises full dataset or $\mathcal{D}_r$ such as Fine Tuning, Amnesiac Unlearning and Fisher forgetting have relatively high execution time. iii) Unlearning methods that utilise only $\mathcal{D}_u$ such as Boundary Unlearning shows a lower execution time. iv) Our solution has the lowest execution time (16x - 1200x lower).

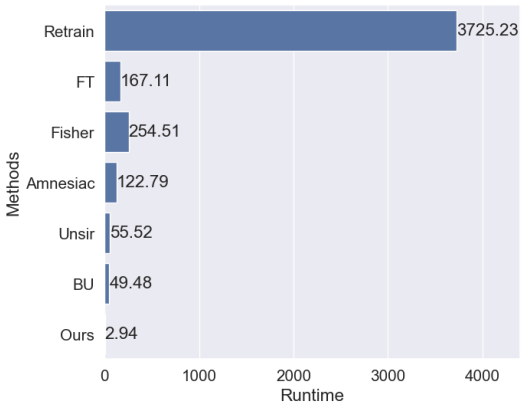

Figure 4: The runtime(s) of each unlearning method.

5.3 Ablation Study

In this section, we conduct an ablation study on the effectiveness of our method for different number of passive parties and different privacy-preserving VFL mechanism.

5.3.1 Evaluation for different number of passive parties

Table 4 shows the accuracy of $\mathcal{D}_r$, $\mathcal{D}_u$ and ASR score on one(1) passive party, two(2) passive parties and four(4) passive parties respectively. The results indicate that our method can perform well in unlearning effectiveness and utility.

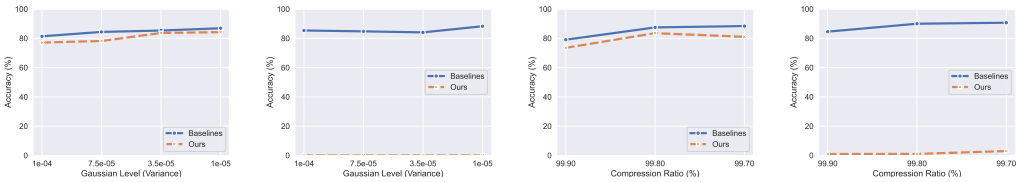

(a) (b) (c) (d)

Figure 6: Comparison of the utility and unlearning effectiveness for Differential Privacy and Gradient Compression privacy preserving VFL methods (Fu et al., 2022b). (a) and (b) show the accuracy of $\mathcal{D}_r$ and $\mathcal{D}_u$ between baseline and our solution on different level of Gaussian Noise model, respectively. While (c) and (d) show the accuracy of $\mathcal{D}_r$ and $\mathcal{D}_u$ between baseline and our solution on different level of gradient compression ratio model, respectively.

5.3.2 Evaluation on different size of D_p

We apply the gradient ascent with different size D_p to achieve unlearning in Fig. 5, e.g, three methods (GA-A using 5000 samples, GA-S using 40 samples and ours). It shows that i) 40 samples is not enough to unlearn since the unlearning result on D_u remains at 40.48% while GA-A with 5000 samples achieves 0%. Meanwhile, ii) our method with only 40 samples able to achieve 0% unlearning effectiveness on D_u.

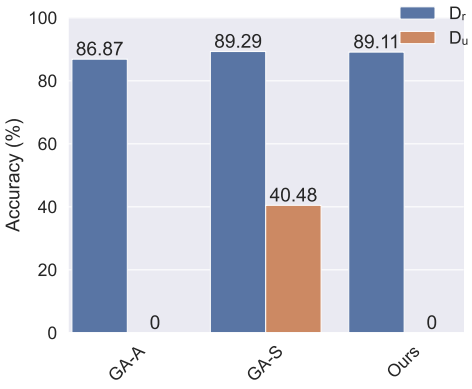

Figure 5: Comparison of the utility and unlearning effectiveness on different size of D_p. The results indicate that when using a limited amount of data ($|D_p| = 40$), directly applying gradient ascent (GA-S) does not achieve satisfactory unlearning effectiveness, as the accuracy on the unlearned data remains at 40.48%. In contrast, our method, which incorporates manifold mixup, demonstrates significantly better unlearning effectiveness. For instance, with only 40 labeled data points, our approach reduces the unlearned accuracy to 0%.

5.3.3 Evaluation for different privacy preserving VFL methods

We evaluate our unlearning methods under two privacy preserving VFL methods: (i) Differential Privacy (Fu et al., 2022b) and (ii) Gradient Compression (Fu et al., 2022b). Fig. 6 presents the effectiveness of our solution on both methods across different levels of variance Gaussian noise and compression ratio, respectively. It shows that even for a large compression ratio and noise level, our proposed method still able to unlearn effectively while the utility of the vertical training decreases significantly.

6 Conclusions

In conclusion, this paper presents a pioneering approach to label unlearning within VFL domain, addressing a critical gap in the existing literature. By introducing a few-shot unlearning method that leverages manifold mixup, we effectively mitigate the risk of label privacy leakage while ensuring efficient unlearning from both active and passive models. Our systematic exploration of potential label privacy risks and extensive experimental validation on benchmark datasets underscores the proposed method's efficacy and rapid performance. Ultimately, this work not only advances the understanding of unlearning in VFL but also sets the stage for further innovations in privacy-preserving collaborative machine learning practices.

REFERENCES

Ali Abbasi, Chayne Thrash, Elaheh Akbari, Daniel Zhang, and Soheil Kolouri. Covarnav: Machine unlearning via model inversion and covariance navigation, 2023. URL https://arxiv.org/abs/2311.12999.

Manaar Alam, Hithem Lamri, and Michail Maniatakos. Get rid of your trail: Remotely erasing backdoors in federated learning, 2023. URL https://arxiv.org/abs/2304.10638.

Lucas Bourtoule, Varun Chandrasekaran, Christopher A. Choquette-Choo, Hengrui Jia, Adelin Travers, Baiwu Zhang, David Lie, and Nicolas Papernot. Machine unlearning, 2020. URL https://arxiv.org/abs/1912.03817.

Xiaoyu Cao, Jinyuan Jia, Zaixi Zhang, and Neil Zhenqiang Gong. Fedrecover: Recovering from poisoning attacks in federated learning using historical information, 2022. URL https://arxiv.org/abs/2210.10936.

Yinzhi Cao and Junfeng Yang. Towards making systems forget with machine unlearning. In *2015 IEEE Symposium on Security and Privacy*, pp. 463–480, 2015. doi: 10.1109/SP.2015.35.

Jiaao Chen, Zichao Yang, and Diyi Yang. Mixtext: Linguistically-informed interpolation of hidden space for semi-supervised text classification, 2020. URL https://arxiv.org/abs/2004.12239.

Min Chen, Zhikun Zhang, Tianhao Wang, Michael Backes, Mathias Humbert, and Yang Zhang. When machine unlearning jeopardizes privacy. In *Proceedings of the 2021 ACM SIGSAC Conference on Computer and Communications Security*, CCS '21. ACM, November 2021. doi: 10.1145/3460120.3484756. URL http://dx.doi.org/10.1145/3460120.3484756.

Min Chen, Weizhuo Gao, Gaoyang Liu, Kai Peng, and Chen Wang. Boundary unlearning, 2023. URL https://arxiv.org/abs/2303.11570.

Dasol Choi and Dongbin Na. Towards machine unlearning benchmarks: Forgetting the personal identities in facial recognition systems, 2023. URL https://arxiv.org/abs/2311.02240.

Vikram S Chundawat, Ayush K Tarun, Murari Mandal, and Mohan Kankanhalli. Can bad teaching induce forgetting? unlearning in deep networks using an incompetent teacher, 2023. URL https://arxiv.org/abs/2205.08096.

Zihao Deng, Zhaoyang Han, Chuan Ma, Ming Ding, Long Yuan, Chunpeng Ge, and Zhe Liu. Vertical federated unlearning on the logistic regression model. *Electronics*, 12(14), 2023. ISSN 2079-9292. doi: 10.3390/electronics12143182. URL https://www.mdpi.com/2079-9292/12/14/3182.

Akash Dhasade, Yaohong Ding, Song Guo, Anne marie Kermarrec, Martijn De Vos, and Leijie Wu. Quickdrop: Efficient federated unlearning by integrated dataset distillation, 2023. URL https://arxiv.org/abs/2311.15603.

Jack Foster, Stefan Schoepf, and Alexandra Brintrup. Fast machine unlearning without retraining through selective synaptic dampening, 2023. URL https://arxiv.org/abs/2308.07707.

Chong Fu, Xuhong Zhang, Shouling Ji, Jinyin Chen, Jingzheng Wu, Shanqing Guo, Jun Zhou, Alex X. Liu, and Ting Wang. Label inference attacks against vertical federated learning. In *31st USENIX Security Symposium (USENIX Security 22)*, pp. 1397–1414, Boston, MA, August 2022a. USENIX Association. ISBN 978-1-939133-31-1. URL https://www.usenix.org/conference/usenixsecurity22/presentation/fu-chong.

Chong Fu, Xuhong Zhang, Shouling Ji, Jinyin Chen, Jingzheng Wu, Shanqing Guo, Jun Zhou, Alex X Liu, and Ting Wang. Label inference attacks against vertical federated learning. In *31st USENIX security symposium (USENIX Security 22)*, pp. 1397–1414, 2022b.

Xiangshan Gao, Xingjun Ma, Jingyi Wang, Youcheng Sun, Bo Li, Shouling Ji, Peng Cheng, and Jiming Chen. Verifi: Towards verifiable federated unlearning, 2022. URL https://arxiv.org/abs/2205.12709.

Sanjam Garg, Shafi Goldwasser, and Prashant Nalini Vasudevan. Formalizing data deletion in the context of the right to be forgotten, 2020. URL https://arxiv.org/abs/2002.10635.

Shashwat Goel, Ameya Prabhu, Amartya Sanyal, Ser-Nam Lim, Philip Torr, and Ponnurangam Kumaraguru. Towards adversarial evaluations for inexact machine unlearning, 2023. URL https://arxiv.org/abs/2201.06640.

Aditya Golatkar, Alessandro Achille, and Stefano Soatto. Eternal sunshine of the spotless net: Selective forgetting in deep networks, 2020a. URL https://arxiv.org/abs/1911.04933.

Aditya Golatkar, Alessandro Achille, and Stefano Soatto. Forgetting outside the box: Scrubbing deep networks of information accessible from input-output observations, 2020b. URL https://arxiv.org/abs/2003.02960.

Aditya Golatkar, Alessandro Achille, Avinash Ravichandran, Marzia Polito, and Stefano Soatto. Mixed-privacy forgetting in deep networks, 2021. URL https://arxiv.org/abs/2012.13431.

Laura Graves, Vineel Nagisetty, and Vijay Ganesh. Amnesiac machine learning, 2020. URL https://arxiv.org/abs/2010.10981.

Hanlin Gu, Jiahuan Luo, Yan Kang, Lixin Fan, and Qiang Yang. Fedpass: privacy-preserving vertical federated deep learning with adaptive obfuscation. In *Proceedings of the Thirty-Second International Joint Conference on Artificial Intelligence*, pp. 3759–3767, 2023.

Hanlin Gu, WinKent Ong, Chee Seng Chan, and Lixin Fan. Ferrari: Federated feature unlearning via optimizing feature sensitivity, 2024a. URL https://arxiv.org/abs/2405.17462.

Hanlin Gu, Gongxi Zhu, Jie Zhang, Xinyuan Zhao, Yuxing Han, Lixin Fan, and Qiang Yang. Unlearning during learning: An efficient federated machine unlearning method, 2024b. URL https://arxiv.org/abs/2405.15474.

Chuan Guo, Tom Goldstein, Awni Hannun, and Laurens van der Maaten. Certified data removal from machine learning models, 2023. URL https://arxiv.org/abs/1911.03030.

Anisa Halimi, Swanand Kadhe, Ambrish Rawat, and Nathalie Baracaldo. Federated unlearning: How to efficiently erase a client in fl?, 2023. URL https://arxiv.org/abs/2207.05521.

Kaiming He, Xiangyu Zhang, Shaoqing Ren, and Jian Sun. Deep residual learning for image recognition, 2015. URL https://arxiv.org/abs/1512.03385.

Tuan Hoang, Santu Rana, Sunil Gupta, and Svetha Venkatesh. Learn to unlearn for deep neural networks: Minimizing unlearning interference with gradient projection, 2023. URL https://arxiv.org/abs/2312.04095.

Hanxun Huang, Xingjun Ma, Sarah Monazam Erfani, James Bailey, and Yisen Wang. Unlearnable examples: Making personal data unexploitable, 2021. URL https://arxiv.org/abs/2101.04898.

Jinghan Jia, Jiancheng Liu, Parikshit Ram, Yuguang Yao, Gaowen Liu, Yang Liu, Pranay Sharma, and Sijia Liu. Model sparsity can simplify machine unlearning, 2024. URL https://arxiv.org/abs/2304.04934.

Alex Krizhevsky, Geoffrey Hinton, et al. Learning multiple layers of features from tiny images. 2009.

Meghdad Kurmanji, Peter Triantafillou, Jamie Hayes, and Eleni Triantafillou. Towards unbounded machine unlearning, 2023. URL https://arxiv.org/abs/2302.09880.

Y. Lecun, L. Bottou, Y. Bengio, and P. Haffner. Gradient-based learning applied to document recognition. *Proceedings of the IEEE*, 86(11):2278–2324, 1998. doi: 10.1109/5.726791.

Guanghao Li, Li Shen, Yan Sun, Yue Hu, Han Hu, and Dacheng Tao. Subspace based federated unlearning, 2023. URL https://arxiv.org/abs/2302.12448.

Li Li, Yuxi Fan, Mike Tse, and Kuo-Yi Lin. A review of applications in federated learning. *Computers & Industrial Engineering*, 149:106854, 2020.

Yi Liu, Lei Xu, Xingliang Yuan, Cong Wang, and Bo Li. The right to be forgotten in federated learning: An efficient realization with rapid retraining. In *IEEE INFOCOM 2022 - IEEE Conference on Computer Communications*. IEEE, May 2022. doi: 10.1109/infocom48880.2022.9796721. URL http://dx.doi.org/10.1109/INFOCOM48880.2022.9796721.

Ziyao Liu, Yu Jiang, Jiyuan Shen, Minyi Peng, Kwok-Yan Lam, Xingliang Yuan, and Xiaoning Liu. A survey on federated unlearning: Challenges, methods, and future directions, 2024. URL https://arxiv.org/abs/2310.20448.

Josh Patterson and Adam Gibson. *Deep Learning: A Practitioner's Approach*. O'Reilly Media, Inc., 1st edition, 2017. ISBN 1491914254.

Nicolò Romandini, Alessio Mora, Carlo Mazzocca, Rebecca Montanari, and Paolo Bellavista. Federated unlearning: A survey on methods, design guidelines, and evaluation metrics, 2024. URL https://arxiv.org/abs/2401.05146.

Reza Shokri, Marco Stronati, Congzheng Song, and Vitaly Shmatikov. Membership inference attacks against machine learning models, 2017. URL https://arxiv.org/abs/1610.05820.

Karen Simonyan and Andrew Zisserman. Very deep convolutional networks for large-scale image recognition, 2015. URL https://arxiv.org/abs/1409.1556.

Ningxin Su and Baochun Li. Asynchronous federated unlearning. In *IEEE INFOCOM 2023 - IEEE Conference on Computer Communications*, pp. 1–10, 2023. doi: 10.1109/INFOCOM53939.2023.10229075.

Ayush K. Tarun, Vikram S. Chundawat, Murari Mandal, and Mohan Kankanhalli. Fast yet effective machine unlearning. *IEEE Transactions on Neural Networks and Learning Systems*, pp. 1–10, 2024. ISSN 2162-2388. doi: 10.1109/tnnls.2023.3266233. URL http://dx.doi.org/10.1109/TNNLS.2023.3266233.

Vikas Verma, Alex Lamb, Christopher Beckham, Amir Najafi, Ioannis Mitliagkas, David Lopez-Paz, and Yoshua Bengio. Manifold mixup: Better representations by interpolating hidden states. In *International conference on machine learning*, pp. 6438–6447. PMLR, 2019.

Junxiao Wang, Song Guo, Xin Xie, and Heng Qi. Federated unlearning via class-discriminative pruning, 2022. URL https://arxiv.org/abs/2110.11794.

Pengfei Wang, Zhaohong Yan, Mohammad S. Obaidat, Zhiwei Yuan, Leyou Yang, Junxiang Zhang, Zongzheng Wei, and Qiang Zhang. Edge caching with federated unlearning for low-latency v2x communications. *IEEE Communications Magazine*, pp. 1–7, 2023. doi: 10.1109/MCOM.001.2300272.

Zichen Wang, Xiangshan Gao, Cong Wang, Peng Cheng, and Jiming Chen. Efficient vertical federated unlearning via fast retraining. *ACM Trans. Internet Technol.*, 24(2), may 2024. ISSN 1533-5399. doi: 10.1145/3657290. URL https://doi.org/10.1145/3657290.

Chen Wu, Sencun Zhu, and Prasenjit Mitra. Federated unlearning with knowledge distillation, 2022. URL https://arxiv.org/abs/2201.09441.

Zhirong Wu, Shuran Song, Aditya Khosla, Fisher Yu, Linguang Zhang, Xiaoou Tang, and Jianxiong Xiao. 3d shapenets: A deep representation for volumetric shapes, 2015. URL https://arxiv.org/abs/1406.5670.

Hui Xia, Shuo Xu, Jiaming Pei, Rui Zhang, Zhi Yu, Weitao Zou, Lukun Wang, and Chao Liu. Fedme2: Memory evaluation & erase promoting federated unlearning in dtmn. *IEEE Journal on Selected Areas in Communications*, 41(11):3573–3588, 2023. doi: 10.1109/JSAC.2023.3310049.

Haonan Yan, Xiaoguang Li, Ziyao Guo, Hui Li, Fenghua Li, and Xiaodong Lin. Arcane: An efficient architecture for exact machine unlearning. In Lud De Raedt (ed.), *Proceedings of the Thirty-First International Joint Conference on Artificial Intelligence, IJCAI-22*, pp. 4006–4013. International Joint Conferences on Artificial Intelligence Organization, 7 2022. doi: 10.24963/ijcai.2022/556. URL https://doi.org/10.24963/ijcai.2022/556. Main Track.

Qiang Yang, Yang Liu, Tianjian Chen, and Yongxin Tong. Federated machine learning: Concept and applications. *ACM Transactions on Intelligent Systems and Technology (TIST)*, 10(2):1–19, 2019.

Guanhua Ye, Tong Chen, Quoc Viet Hung Nguyen, and Hongzhi Yin. Heterogeneous decentralized machine unlearning with seed model distillation, 2023. URL https://arxiv.org/abs/2308.13269.

Wei Yuan, Hongzhi Yin, Fangzhao Wu, Shijie Zhang, Tieke He, and Hao Wang. Federated unlearning for on-device recommendation, 2022. URL https://arxiv.org/abs/2210.10958.

Jian Zhang, Bowen Li Jie Li, and Chentao Wu. Securecut: Federated gradient boosting decision trees with efficient machine unlearning, 2023a. URL https://arxiv.org/abs/2311.13174.

Lefeng Zhang, Tianqing Zhu, Haibin Zhang, Ping Xiong, and Wanlei Zhou. Fedrecovery: Differentially private machine unlearning for federated learning frameworks. *IEEE Transactions on Information Forensics and Security*, 18:4732–4746, 2023b. doi: 10.1109/TIFS.2023.3297905.

Xulong Zhang, Jianzong Wang, Ning Cheng, Yifu Sun, Chuanyao Zhang, and Jing Xiao. Machine unlearning methodology base on stochastic teacher network, 2023c. URL https://arxiv.org/abs/2308.14322.

Yang Zhao, Jiaxi Yang, Yiling Tao, Lixu Wang, Xiaoxiao Li, and Dusit Niyato. A survey of federated unlearning: A taxonomy, challenges and future directions, 2024a. URL https://arxiv.org/abs/2310.19218.

Yian Zhao, Pengfei Wang, Heng Qi, Jianguo Huang, Zongzheng Wei, and Qiang Zhang. Federated unlearning with momentum degradation. *IEEE Internet of Things Journal*, 11(5):8860–8870, 2024b. doi: 10.1109/JIOT.2023.3321594.

Tianyuan Zou, Yang Liu, Yan Kang, Wenhan Liu, Yuanqin He, Zhihao Yi, Qiang Yang, and Ya-Qin Zhang. Defending batch-level label inference and replacement attacks in vertical federated learning. *IEEE Transactions on Big Data*, 2022.

A APPENDIX

This section provides a detailed information on our experimental settings and additional experimental results.

A.1 PROOF OF THEOREM

Consider a scenario where the active party seeks to unlearn the label y' with the corresponding feature x' and embedding $H' = G_\theta(x')$. The gradient ascent approach aims to remove the label information y' from both the active model θ and the passive model ω.

1) **Unlearning effectiveness for Gradient Ascent (GA).** Using the first-order Taylor expansion of $\ell(\omega; H', y')$ around the initial parameter ω_t, we obtain:

$$\ell(\omega_{t+1}; H', y') \approx \ell(\omega_t; H', y') + \nabla_\omega \ell(\omega_t; H', y')^\top (\omega_{t+1} - \omega_t).$$

Substituting the gradient ascent update $\omega_{t+1} = \omega_t + \eta \nabla_\omega \ell(\omega_t; H', y')$ (as defined in Eq. (5) of the main text), this becomes:

$$\ell(\omega_{t+1}; H', y') \approx \ell(\omega_t; H', y') + \eta \|\nabla_\omega \ell(\omega_t; H', y')\|^2.$$

Since $\eta > 0$, the loss $\ell(\omega; H', y')$ increases with each gradient ascent step, effectively reducing the contribution of the label y' to the active model ω. Similarly, for the passive model θ, we derive:

$$\begin{aligned}
\ell(\theta_{t+1}; x', y') &\approx \ell(\theta_t; x', y') + \nabla_\theta \ell(\theta_t; x', y')^\top (\theta_{t+1} - \theta_t) \\
&= \ell(\theta_t; x', y') + \eta \nabla_\theta \ell(\theta_t; x', y')^\top (\nabla_H \ell \nabla_\theta H) \\
&= \ell(\theta_t; x', y') + \eta \|\nabla_\theta \ell(\theta_t; x', y')\|^2,
\end{aligned}$$

where the first equation is due to the Eq. (6) of the main text and second equation is according to the chain rule. Thus, the contribution of the label y' is effectively removed from the passive model θ.

2) *If the loss function ℓ is β-smooth*, we can further derive:

$$\begin{aligned}
&\|\nabla_\omega \ell(\omega_T; H', y')\| \leq \beta \|\omega_T - \omega_0\| \\
&= \|\sum_{t=0}^{T-1} \nabla_\omega \ell(\omega_t; H', y')\| \leq \beta\eta \sum_{t=0}^{T-1} \|\nabla_\omega \ell(\omega_t; H', y')\|,
\end{aligned} \tag{7}$$

where the second equation follows from Eq. (5) in the main text. **This result indicates that the convergence of gradient ascent depends on the learning rate** η. For instance, when the learning rate is small or includes a weight decay strategy(Patterson & Gibson, 2017), such as $\eta < \frac{1}{2\beta T}$, the gradient norm $\|\nabla_\omega \ell(\omega_T; H', y')\|$ tends to zero.

It is important to note that gradient ascent may impact the model utility on the remained data. To mitigate this, a small learning rate (smaller than e^{-6} in Table 7 and 8) is adopted in this paper to minimize any decline in model utility for the remained data D_r. The experimental results presented in Section 5 validate this approach.

3) **The gradient ascent strategy aims to increase the model's loss corresponding to the unlearned label** y', thereby eliminating the contribution of the unlearned label y' to the model, as illustrated in 1).

A.2 TABLE OF NOTATION

Table 5 summarises all the notations used in this paper.

A.3 EXPERIMENTAL SETUP

Datasets *MNIST*(Lecun et al., 1998) datasets contain images of handwritten digits. MNIST dataset comprises 60,000 training examples and 10,000 test examples. Each example is represented as a single-channel image with dimensions of 28x28 pixels, categorised into one of 10 classes. *CIFAR10* (Krizhevsky et al., 2009) dataset comprises 60,000 images, each with dimensions of 32x32

Notation	Meaning
F_ω, G_{θ_k}	Active model and k_{th} passive model
K	The number of passive party
λ	Mixed coefficient
η	Learning rate
N	Unlearning epochs
$\mathbf{x}_k$	Private features own by k_{th} passive party
y	Private label own by active party
y^u	The unlearn labels
$\{x_k^u\}$	The unlearned feature for client k corresponding to the y^u
x_k^p	The known features for client k corresponding to the y^u
H_k	Forward embedding of passive party k
H_k'	Augmented forward embedding of passive party k
g_k'	Gradient on the embedding H_k'.

Table 5: Table of Notations

pixels and three colour channels, distributed across 10 classes. This dataset includes 6,000 images per class and is partitioned into 50,000 training examples and 10,000 test examples. Within each class, there are 5000 training images and 1000 test images. Similarly, the *CIFAR100* (Krizhevsky et al., 2009) dataset shares the same image dimensions and structure as CIFAR10 but extends to 100 classes, with each class containing 600 images. Within each class, there are 500 training images and 100 test images. *ModelNet* (Wu et al., 2015) dataset is a widely-used 3D shape classification and shape retrieval benchmark, which currently contains 127,915 3D CAD models from 662 object categories. For the MNIST, CIFAR10, and CIFAR100 datasets, each image feature is divided among K parties, where K represents the number of passive parties. For the ModelNet dataset, we generate K 2D multi-view images per 3D mesh model by placing two virtual cameras evenly distributed around the centroid. Each passive party is assigned one of the K generated 2D multi-view images.

Baselines The baseline methods used in the paper includes:

Baseline: Th original model before unlearning.

Retrain: Retrain the model from scratch with $\mathcal{D}_r$ with the same hyper-parameters to baseline.

Fine Tuning(Golatkar et al., 2020a; Jia et al., 2024): The baseline model is fine-tuned using $\mathcal{D}_r$ for 5 epochs with 0.01 learning rate.

Fisher Forgetting(Golatkar et al., 2020a): We use fisher information matrix(FIM) to inject noise into the parameters proportional to their relative importance to the $\mathcal{D}_f$ compared to the $\mathcal{D}_r$.

Amnesiac(Graves et al., 2020): We retrain the model for 3 epochs with relabeled $\mathcal{D}_f$ with incorrect random label and $\mathcal{D}_r$.

Unsir(Tarun et al., 2024): We introduce noise matrix on $\mathcal{D}_f$ to impair the model with noise generated and repair the model with $\mathcal{D}_r$.

Boundary Unlearning(Chen et al., 2023): We create adversarial examples from $\mathcal{D}_f$ and assign new nearest incorrect adversarial label to shrink the $\mathcal{D}_f$ to nearest incorrect decision boundary.

Gradient Ascent(Golatkar et al., 2020a): We maximise the loss of $\mathcal{D}_f$ on the model for small number of epochs.

Model Architecture Table 6 summarised our VFL framework settings.

Model name	Model of Passive Party	Model of Active Party
Resnet18	20 Conv	1 FC
Vgg16	13 Conv	3 FC

Table 6: Models in experiments. FC: Fully-connected layer. Conv: convolutional layer

Implementation Details Table 7 and 8 summarise the hyper-parameters for our unlearning method.

Hyper-parameters	Single-class					
	Resnet18-MNIST	Resnet18-CIFAR10	Resnet18-CIFAR100	Resnet18-ModelNet	Vgg16-CIFAR10	Vgg16-CIFAR100
Optimization Method	SGD	SGD	SGD	SGD	SGD	SGD
Unlearning Rate	2e-7	2e-7	5e-7	5e-7	2e-7	5e-7
Unlearning Epochs	10	15	7	4	15	7
Number of Data Samples	40	40	30	30	40	30
Batch Size	32	32	32	32	32	32
Weight Decay	5e-4	5e-4	5e-4	5e-4	5e-4	5e-4
Momentum	0.9	0.9	0.9	0.9	0.9	0.9

Table 7: Hyper-parameters use for unlearning in our solution in Single-class unlearning.

Hyper-parameters	Two-classes				Multi-classes	
	Resnet18-CIFAR10	Resnet18-CIFAR100	Vgg16-CIFAR10	Vgg16-Cifar100	Resnet18-CIFAR100	Vgg16-CIFAR100
Optimization Method	SGD	SGD	SGD	SGD	SGD	SGD
Unlearning Rate	1e-6	9e-7	1e-6	9e-7	9e-7	9e-7
Unlearning Epochs	15	10	15	5	15	5
Number of Data Samples	40	20	40	20	15	15
Batch Size	32	32	32	32	32	32
Weight Decay	5e-4	5e-4	5e-4	5e-4	5e-4	5e-4
Momentum	0.9	0.9	0.9	0.9	0.9	0.9

Table 8: Hyper-parameters use for unlearning in our solution in two-classes and multi-classes unlearning.

Table 9 summarises the model name, datasets and unlearn classes involve in each unlearning scenarios.

Scenarios	Models	Datasets	Unlearn Classes
Single-class Unlearning	Resnet18	MNIST, CIFAR10, CIFAR100, ModelNet	0
	Vgg16	CIFAR10, CIFAR100	0
Two-classes Unlearning	Resnet18	CIFAR10, CIFAR100	0, 2
	Vgg16	CIFAR10, CIFAR100	0, 2
Multi-classes Unlearning	Resnet18	CIFAR100	0, 2, 5, 7
	Vgg16	CIFAR100	0, 2, 5, 7

Table 9: Models and datasets involve in each unlearning scenarios.

For each dataset used in this paper, we augment the embeddings with two coefficients, i.e., $\lambda = 0.25$ and $\lambda = 0.5$. Additionally, we evaluate the impact of different λ values in Table 10. The results indicate that variations in λ have a minimal impact on the unlearning effectiveness.

λ Rate	Metrics	Accuracy (%)
[0.2, 0.5]	$\mathcal{D}_r$	88.69 ± 0.19
	$\mathcal{D}_u$	1.77 ± 0.57
[0.25, 0.5]	$\mathcal{D}_r$	89.11 ± 0.14
	$\mathcal{D}_u$	0.00 ± 0.00
[0.33, 0.5]	$\mathcal{D}_r$	88.78 ± 0.09
	$\mathcal{D}_u$	2.10 ± 0.42

Table 10: Different lambda rate on single-label unlearning scenarios on CIFAR10 dataset with ResNet18 architecture. We unlearn label 0 in this experiment.

A.4 Additional Experiments Results

We have incorporated one experiment using a healthcare dataset for classification task, specifically the Brain Tumor MRI dataset (Wang et al., 2024), which is commonly used in healthcare scenarios. The Brain Tumor MRI dataset consists of 7,023 human brain MRI images categorized into four classes: glioma, meningioma, no tumor, and pituitary.

Table 11 demonstrates that our method achieves strong unlearning effectiveness, with the accuracy on unlearned data (D_u) dropping from 95.67% to 2.43%. Furthermore, the accuracy on the remained data (D_r) outperforms other unlearning methods, except for retraining. For instance, the Amnesiac method results in an accuracy drop exceeding 20% while our method drops less than 10%. The decrease in the remained data accuracy for our method is attributed to the similarity of features among different labels. Removing one label can inadvertently impact the utility of other labels when using the gradient ascent method. In contrast, the retraining method performs well in maintaining the utility of other labels; however, it is significantly more time-consuming.

Metrics	Accuracy (%)						
	Baselines	Retrain	FT	Fisher	Amnesiac	BU	Ours
$\mathcal{D}_r$	97.92	98.81 ± 0.34	81.89 ± 0.82	30.26 ± 0.21	73.29 ± 0.09	45.30 ± 0.91	**89.05 ± 0.61**
$\mathcal{D}_u$	95.67	0.00 ± 0.00	4.33 ± 0.49	**0.00 ± 0.00**	**0.00 ± 0.00**	3.67 ± 0.14	2.43 ± 0.04

Table 11: Single-label unlearning scenario with Brain MRI datasets on ResNet18 architecture. This experiments have one active party and two passive parties. The image features is split to half and each passive party own half of the image features. We unlearn label 0 (glioma) in this experiments.

Also, we have added experiments on Non-vision dataset (Yahoo Answers dataset (Fu et al., 2022a)) for the classification task. Yahoo Answers is a dataset designed for text classification tasks, comprising 10 classes (topics) such as "Society & Culture," "Science & Mathematics," "Health," "Education & Reference," among others. Each class contains 140,000 training samples and 6,000 testing samples. For simplicity, we utilized 5,000 training samples and 2,000 testing samples from each class.

Table 12 illustrates that our method performs effectively on both the accuracy of the remained data and the unlearned data. For instance, the unlearned data accuracy decreases from 41.63% to 5.14%, while the accuracy drop on the remained data is less than 3%.

Metrics	Accuracy (%)		
	Baseline	Retrain	Ours
$\mathcal{D}_r$	62.92	63.14 ± 0.45	60.72 ± 0.98
$\mathcal{D}_u$	41.63	0.00 ± 0.00	5.14 ± 1.04

Table 12: Single-label unlearning scenario on Yahoo Answer datasets with MixText architecture ((Chen et al., 2020), transformer-based models). This experiments have one active party and two passive parties. Each sample (a single paragraph of text) is divided into two paragraphs, with each passive party holding one of them. We unlearn label 6 (Business & Finance) in this experiments.

In addition, we conducted experiments with one active party and eight passive parties on the CIFAR-10 dataset using the ResNet-18 architecture. The image features were split into eight parts, with each passive party owning one-eighth of the image features. Table 13 demonstrates that the proposed method continues to perform well in terms of both unlearning effectiveness and the utility of the remained data. For instance, the accuracy on the unlearned data drops to 0.17%, while the accuracy on the remained data decreases by less than 3%.

Metrics	Accuracy (%)						
	Baseline	Retrain	Fisher	Amnesiac	Unsir	BU	Ours
$\mathcal{D}_r$	84.16	84.98 ± 0.11	18.01 ± 0.38	77.28 ± 0.93	67.95 ± 0.86	70.99 ± 0.70	82.72 ± 0.99
$\mathcal{D}_u$	87.9	0.00 ± 0.00	0.00 ± 0.00	0.00 ± 0.00	0.00 ± 0.00	0.50 ± 0.07	0.17 ± 0.03

Table 13: Single-label unlearning scenario on CIFAR10 dataset with Resnet18 architecture on 8 passive parties. The image features is equally split into 8 parts and each passive party own one eight of the image features. We unlearn label 0 in this experiment.

Figure 8 shows MIA graphs for various number of passive parties. Moreover, Figure 7 shows the PMC attack (one strongest label privacy attack in (Fu et al., 2022b)) before and after unlearning methods. It demonstrates that our methods achieve beyond 40% drops for the model accuracy on D_u.

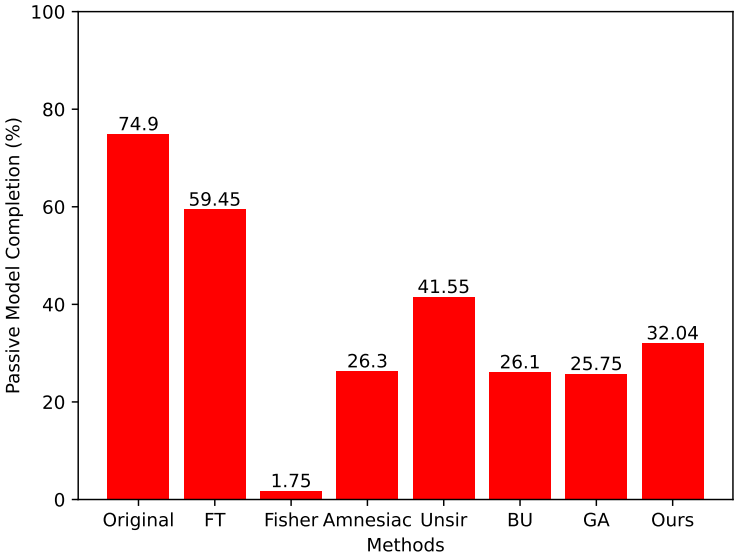

Figure 7: PMC resnet18 cifar10 single class

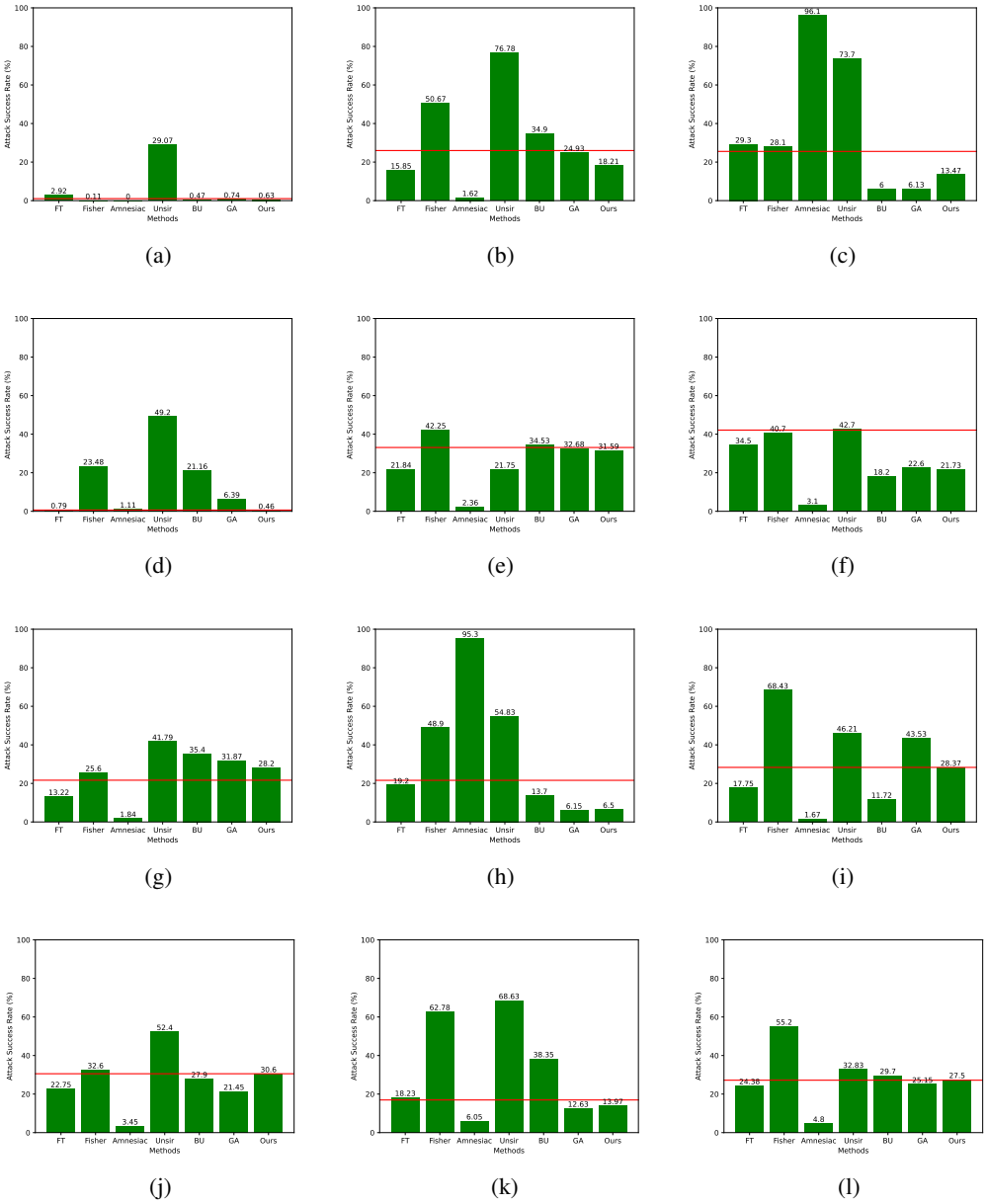

Figure 8: The following sub-figures show the MIA attack success rate on (a) Single-class Resnet18 Mnist, (b) Single-class Resnet18 Cifar10, (c) Single-class Resnet18 Cifar100, (d) Single-class Resnet18 ModelNet, (e) Single-class Vgg16 Cifar10, (f) Single-class Vgg16 Cifar100, (g) Two-classes Resnet18 Cifar10, (h) Two-classes Resnet18 Cifar100, (i) Two-classes Vgg16 Cifar10, (j) Two-classes Vgg16 Cifar100, (k) Multi-classes Resnet18 Cifar100, (l) Multi-classes Vgg16 Cifar100. The red line in graphs represent the ASR of retrained model.